CrossMark

ORIGINAL ARTICLE

Poisson noise removal of images on graphs using tight wavelet frames

Cong Wang[1] · **Jianbin Yang**[1]

Abstract After many years of study, the subject of image denoising on the flat domain is well developed. However, many practical problems arising from different areas, such as computer vision, computer graphics, geometric modeling and medical imaging, involve images on the irregular domain sets such as graphs. In this paper, we consider Poisson and mixed Poisson–Gaussian noise removal of images on graphs. Based on the statistical characteristic of the observed noisy images, we propose a wavelet frame-based variational model to restore images on graphs. The model contains a weighted ℓ_2 fidelity term and an ℓ_1-regularized term which makes additional use of the tight wavelet frame transform on graphs in order to preserve key features such as textures and edges of images. We then apply the popular alternating direction method of multipliers (ADMM) to solve the model. Finally, we provide supporting numerical experiments on graphs and compare with other denoising methods. The results on some image denoising tasks indicate the effectiveness of our method.

Keywords Images on graphs · Tight wavelet frames · Poisson noise · Mixed Poisson–Gaussian noise

1 Introduction

In recent years, many interesting scientific problems have increasingly involved analyzing and manipulating structured data. Such data often consist of sampled real-valued functions defined on some irregular domain sets such as graphs. As many traditional methods for signal processing are designed for data defined on regular Euclidean spaces, such as image and video processing, the development of mathematical tools and methods that are able to accommodate complicated data domains is also an important topic. In practical applications, many data sets such as mesh surfaces, point clouds and data defined on network-like structures can naturally be modeled as scalar functions defined on the vertices of graphs, which are generally considered as a certain discretization or random samples from some Riemannian manifold [1,10,16,19,31,37].

Image processing on the graph domain is interesting, for it arises in many practical applications and provides new insights in signal processing (see e.g. [12,25,38]). Graphs provide a flexible generalization of regular Euclidean domain and surface domain [2,4,15,20,28,35,37], and they can approximate arbitrary topology and geometry structure. For example, Niyobuhungiro et al. [25] considered an analogue of the well-known ROF denoising model [28] on a general finite directed and connected graph. Zosso et al. [38] considered a graph-based approach for image segmentation. More recently, Dong [12] introduced a tight wavelet frame transform on graphs and discussed graph data denoising.

A graph is denoted by $G = \{V, E, \omega\}$, where $V := \{v_k : k = 0, \ldots, K - 1\}$ is the set of vertices, $E \subset V \times V$ is the set of edges and $\omega : E \mapsto \mathbb{R}^+$ denotes a weighted function of every two edges. Let $u : V \mapsto \mathbb{R}$ be an image function defined on the graph G, which can be viewed as a vector in $\mathbb{R}^K$. Due to sampling measurements and instruments, sampling noise is inevitable [29]. Thus, a fundamental problem is to remove noise to obtain high-quality images before further processing. Let f_G be an observed image on graph G which is formulated as

✉ Jianbin Yang
jbyang@hhu.edu.cn

Cong Wang
wangc0705@hhu.edu.cn

1 College of Science, Hohai University, Nanjing 211100, China

$$f_G = u + \eta, \tag{1.1}$$

where u is the clean image and η is the perturbation noise. When η in (1.1) is additive white Gaussian noise, it is mostly considered in the early literature for its good characterization of system noise, whereas non-Gaussian type of noise are also encountered in many real observations due to noisy sensors and channel transmission (see e.g. [18]).

An important variant is Poisson noise, which is generally produced by low number of photons, such as fluorescence microscopy, emission tomography. The poisson noise data, i.e., the probability of receiving k particles is given by

$$\mathbf{P}(k) = \frac{e^{-\tau}\tau^k}{k!}, k = 0, 1, 2, \ldots, \tag{1.2}$$

where τ is the expected value and the variance of random counts. When images are defined on Euclidean space, many studies have been made for poisson noise removal in the past decade (see e.g. [9,18,21,22,36]). For example, based on the statistics of Poisson noise, the generalized Kullback–Leibler (KL)-divergence fidelity was used in a variational model for Poisson noise removal [11]. Luisier et al. in [23] constructed a Stein's unbiased risk estimator (SURE) in the wavelet domain for removal of mixed Poisson–Gaussian noise. Gong et al. in [18] proposed a universal $\ell_1 + \ell_2$ fidelity term for mixed or unknown noise removal. Recently, Stagliò et al. [33] and Li et al. [22] studied Poisson noise removal by approximating the generalized KL-divergence in terms of a weighted least-squares function.

The main focus of this paper is to extend Poisson noise removal of images on regular Euclidean space to images defined on graphs. We assume that the observation f_G on graph is corrupted by Poisson noise, i.e.

$$f_G \sim Poisson(u),$$

and the noise on each pixel is independent. Inspired by some recent wavelet frames-based image restoration methodologies (see [8,14,18,22] and the references therein), we propose the following variational model to remove noise:

$$\min_u E(u) := \frac{1}{2} \left\| \frac{u - f_G}{\sqrt{u}} \right\|_{\ell_2(G)}^2 + \lambda \|\mathcal{W}u\|_{\ell_1(G)}. \tag{1.3}$$

Here, the first term can be rewritten as $\frac{1}{2}\|u - f_G\|_{\Sigma^{-1}}^2$, where $\Sigma = \text{diag}(u)$, is a reweighed ℓ_2 fidelity term. This term was first introduced in [22,33] for approximating the KL-divergence fidelity. In practical implement, in order to guarantee the numerical stability, we add a very small positive constant (the fixed background image, see [3,6,30]) to u in model (1.3). The second term is a regularization term, where $\mathcal{W}$ is the tight wavelet frame transform on graphs, $\|\cdot\|_{\ell_1(G)}$ denotes the ℓ_1 vector norm on graphs, and λ is

a positive parameter to balance the two terms. The detailed derivation of model (1.3) will be given in Sect. 3.

The regularization term is designed based on a priori assumption on u. One of the assumptions commonly used is the sparsity of the underlying solutions in the wavelet frame domain [7,8,14,22]. The effectiveness of wavelet tight frames has been proved in many applications in signal and image processing [8,14,18,22], since they are able to sparsely approximate piecewise smooth functions in an efficient way and provide fast decomposition and reconstruction algorithms. We will show that such a simple system can also be used to effectively restore images defined on graphs from noisy data. The extension of image denoising model on flat domain to graph data denoising is not trivial because of the nonlinear nature of the graphs and the corresponding algorithms [12,13]. Furthermore, because of the ℓ_1-norm, the regularization term $\|\mathcal{W}u\|_{\ell_1(G)}$ gives preference to a solution u whose wavelet coefficient sequence is sparse, and to keep the important features of image data such as textures and edges while removing spurious information.

The difficulty for solving (1.3) is the nonlinear nature of the graph domain, and to either approximate or directly solve the weighted square problem involving unknown u in the fidelity term. We are interested in taking advantage of the weighted least square structure and utilizing popular efficient sparse regularization scheme, such as the alternating direction method of multipliers (ADMM) [5,8,17] to solve the model.

The rest of this paper is organized as follows: in Sects. 2.1 and 2.2, we give a brief review of spectral graph theory and the wavelet frame transform on graphs. Next, in Sect. 3.1, we propose a wavelet frame-based variational model for removal of Poisson noise of images on graphs. Then, we present an algorithm to solve the model. In Sect. 3.2, we consider the case of removal of mixed Poisson–Gaussian noise of images on graphs. In the last section, we present some numerical experiments and compare with other denoising methods.

2 Background

2.1 Graph Fourier transform

To understand and analyze the data on graphs, we first review the spectral graph theory, especially the graph Laplacian, which is widely used to reveal the geometric properties of the graph. Let $G := \{V, E, \omega\}$ be a graph, where $V := \{v_k : k = 0, \ldots, K-1\}$ is the set of vertices, $E \subset V \times V$ is the set of edges, and $\omega : E \mapsto \mathbb{R}^+$ denotes a weight function. Here, we choose the following commonly used weight function

$$\omega(v_k, v_{k'}) := e^{-\|v_k - v_{k'}\|_2^2/\rho}, \quad \rho > 0. \tag{2.1}$$

Let $A := (a_{k,k'})$ be the adjacency matrix of G with

$$a_{k,k'} := \begin{cases} \omega(v_k, v_{k'}) & \text{if } v_k \text{ and } v_{k'} \text{ are connected by an edge in } E, \\ 0 & \text{otherwise.} \end{cases}$$

Let $D := \text{diag}\{d[0], d[1], \ldots, d[K-1]\}$ be the degree matrix of G, where $d[k]$ is the degree of node v_k defined by $d[k] := \Sigma_{k'} a_{k,k'}$. Then the (unnormalized) graph Laplacian $\mathcal{L}$ can be defined by the following form

$$\mathcal{L} := D - A.$$

With eigenvalue decomposition, we denote the set of pairs of eigenvalues and eigenfunctions of $\mathcal{L}$ as $\{(\lambda_k, u_k)\}_{k=0}^{K-1}$ with $0 = \lambda_0 < \lambda_1 \leq \lambda_2 \leq \cdots \leq \lambda_{K-1}$. The eigenfunctions form an orthonormal basis for all functions on the graph:

$$\langle u_k, u_{k'} \rangle := \sum_{n=0}^{K-1} u_k[n] u_{k'}[n] = \delta_{k,k'}.$$

Let $f_G : V \mapsto \mathbb{R}$ be a function on the graph G. Then its Fourier transform is defined by

$$\widehat{f_G}[k] := \sum_{n=0}^{K-1} f_G[n] u_k[n], \quad k = 0, 1, \ldots, K-1.$$

2.2 Wavelet frame transform on graphs

Wavelet frames have been proved over the past decade to be an exceptionally useful tool for image denoising, inpainting, function and surface reconstruction, etc. (see [7,8,13,14,22,34,35] and many references therein). Much of the power of wavelet methods comes from their ability to represent both smooth and/or locally bumpy functions in an efficient way and provide time and frequency localization. In this subsection, we introduce wavelet frame transform on graphs. Interested readers should consult [12] for more details.

A countable set $X \subset L_2(\mathbb{R})$ is called a tight frame of $L_2(\mathbb{R})$ if

$$f = \sum_{g \in X} \langle f, g \rangle g, \quad \forall f \in L_2(\mathbb{R}),$$

where $\langle \cdot, \cdot \rangle$ denotes the inner product of $L_2(\mathbb{R})$. A wavelet system $X(\Psi)$ is defined to be a collection of dilations and shifts of a finite set $\Psi := \{\psi_1, \ldots, \psi_r\} \subset L_2(\mathbb{R})$,

$$X(\Psi) := \{\psi_{\ell,j,k} = 2^{j/2} \psi_\ell(2^j \cdot -k), 1 \leq \ell \leq r, j, k \in \mathbb{Z}\}.$$

When $X(\Psi)$ forms a tight frame, it is called a wavelet tight frame.

To construct wavelet tight frames, one usually starts with a refinable function ϕ with a refinement mask a_0 satisfying

$$\phi = 2 \sum_{k \in \mathbb{Z}} a_0[k] \phi(2 \cdot -k).$$

The idea of an MRA-based construction of a wavelet tight frame is to find masks a_ℓ, which are finite sequences, such that

$$\psi_\ell = 2 \sum_{k \in \mathbb{Z}} a_\ell[k] \phi(2 \cdot -k), \quad 1 \leq \ell \leq r.$$

The sequences $a_1, \ldots, a_r$ are the high pass filters of the system, and a_0 is the low pass filter.

The Unitary Extension Principle (UEP) of [26,27] provides a general theory of the construction of tight wavelet frame. Roughly speaking, $X(\Psi)$ forms a tight frame provided that

$$\sum_{\ell=0}^r |\widehat{a_\ell}(\xi)|^2 = 1 \quad \text{and} \quad \sum_{\ell=0}^r \widehat{a_\ell}(\xi) \overline{\widehat{a_\ell}(\xi + \pi)} = 0,$$

where the Fourier series of a_ℓ is denoted as

$$\widehat{a_\ell}(\xi) := \sum_{k \in \mathbb{Z}} a_\ell[k] e^{-ik\xi}.$$

As an application of UEP, a family of wavelet tight frame systems is derived in [26] by using uniform B-splines as the refinable function ϕ. The simplest system in this family is the piecewise linear B-spline frame, where $\phi = B_2 = \max(1 - |x|, 0)$ with the refinement mask $a_0 = \frac{1}{4}[1, 2, 1]$, and $a_1 = \frac{\sqrt{2}}{4}[1, 0, -1]$, $a_2 = \frac{1}{4}[-1, 2, -1]$. Then, the system $X(\{\psi_1, \psi_2\})$ defined in (2.2) is a tight wavelet frame of $L_2(\mathbb{R})$.

For a graph $G := \{V, E, \omega\}$, we formulate function $f_G : V \mapsto \mathbb{R}$ by a K-dimensional vector defined on the vertices. Let $\{\lambda_k : k = 0 \ldots, K-1\}$ be the eigenvalues of $\mathcal{L}$ defined in Sect. 2.1. In the following, we introduce the discrete tight wavelet frame transform of f_G in the Fourier domain.

Let $\{a_\ell : 0 \leq \ell \leq r\}$ be the masks of a tight frame system $X(\Psi)$ and $\widehat{a_\ell^*}$ be the complex conjugate of $\widehat{a_\ell}$. The (undecimated) L-level tight wavelet frame decomposition $\mathcal{W}$ is defined as

$$\mathcal{W} f_G := \{\mathcal{W}_{\ell,p} f_G : 0 \leq \ell \leq r, 1 \leq p \leq L\}$$

with

$$\widehat{\mathcal{W}_{\ell,p} f_G}[k]$$
$$:= \begin{cases} \widehat{a_\ell^*}(2^{-N} \lambda_k) \widehat{f_G}[k] & p = 1 \\ \widehat{a_\ell^*}(2^{-N+p-1} \lambda_k) \widehat{a_0^*}(2^{-N+p-2} \lambda_k) \cdots \widehat{a_0^*}(2^{-N} \lambda_k) \widehat{f_G}[k] & 2 \leq p \leq L. \end{cases}$$
$$(2.2)$$

Here, the index ℓ, $0 \leq \ell \leq r$, denotes the band of the transform, and the index p denotes the level of the transform. The dilation scale N is chosen as the smallest integer such that $\lambda_{\max} := \lambda_{K-1} \leq 2^N \pi$. Note that the scale N is selected such that $2^{-N}\lambda_k \in [0, \pi]$ for $0 \leq k \leq K-1$.

Let $\boldsymbol{\alpha} := \mathcal{W} f_G := \{\alpha_{\ell,p} : 0 \leq \ell \leq r, 1 \leq p \leq L\}$ with $\alpha_{\ell,p} := \mathcal{W}_{\ell,p} f_G$, be the tight wavelet frame coefficients of f_G. We denote the tight wavelet frame reconstruction as $\mathcal{W}^T \boldsymbol{\alpha}$, which is defined by the following iterative procedure

$$\widehat{\alpha}_{0,p-1}[k] = \sum_{\ell=0}^{r} \widehat{a}_\ell(2^{-N+p-1}\lambda_k)\widehat{\alpha}_{\ell,p}[k]$$
$$\text{for } p = L, L-1, \ldots, 1,$$

where $\alpha_{0,0} := \mathcal{W}^T \boldsymbol{\alpha}$ is the reconstructed graph data from $\boldsymbol{\alpha}$. By [12, Theorem 3.1], we have $\mathcal{W}^T \mathcal{W} = \mathcal{I}$, i.e. $\mathcal{W}^T \mathcal{W} f_G = f_G$ for any function f_G defined on graph G.

In practical computations, it is very expensive to obtain the full set of eigenvectors and eigenvalues of the graph Laplacian of large graphs. A solution to such challenge is to approximate masks by Chebyshev polynomials [24,32], so that the eigenvalue decomposition of the graph Laplacian is not needed. The masks a_ℓ, $0 \leq \ell \leq r$, that we use are finitely supported sequences, thus $\widehat{a}_\ell$ are trigonometric polynomials and can be accurately approximated by low-degree Chebyshev polynomials. The Chebyshev polynomial approximation of the mask $\widehat{a}_\ell(\xi)$, $\xi \in [0, \pi]$ can be formulated as

$$\widehat{a}_\ell(\xi) \approx \mathcal{T}_\ell^n(\xi) = \frac{1}{2}c_{\ell,0} + \sum_{k=1}^{n-1} c_{\ell,k} T_k(\xi),$$

where

$$c_{\ell,k} = \frac{2}{\pi} \int_0^\pi \cos(k\theta)\widehat{a}_\ell\left(\frac{\pi}{2}(\cos(\theta)+1)\right) d\theta,$$

and

$$T_k(\xi) = \begin{cases} 1 & k = 0, \\ \dfrac{\xi - \pi/2}{\pi/2} & k = 1, \\ \dfrac{4}{\pi}(\xi - \pi/2)T_{k-1}(\xi) - T_{k-2}(\xi) & k = 2, 3, \ldots. \end{cases}$$

Note that the graph Laplacian $\mathcal{L}$ admits the eigenvalue decomposition $\mathcal{L} = U\Lambda U^T$, where $\Lambda := \mathrm{diag}\{\lambda_0, \lambda_1, \ldots, \lambda_{K-1}\}$ and columns of U are the eigenvectors. Then the wavelet frame transform (2.2) can be rewritten in the matrix form in time domain:

$$\mathcal{W}_{\ell,p} f_G[k]$$
$$:= \begin{cases} U\widehat{\mathbf{a}}_\ell^*(2^{-N}\Lambda)U^T f_G & p = 1 \\ U\widehat{\mathbf{a}}_\ell^*(2^{-N+p-1}\Lambda)\widehat{\mathbf{a}}_0^*(2^{-N+p-2}\Lambda)\cdots\widehat{\mathbf{a}}_0^*(2^{-N}\Lambda)U^T f_G & 2 \leq p \leq L \end{cases},$$

where $\widehat{\mathbf{a}}_\ell^*(\gamma\Lambda) := \mathrm{diag}\{\widehat{a}_\ell^*(\gamma\lambda_0), \widehat{a}_\ell^*(\gamma\lambda_1), \ldots, \widehat{a}_\ell^*(\gamma\lambda_{K-1})\}$. If we substitute $\widehat{a}_\ell$ by polynomial $\mathcal{T}_\ell^n$, then

$$U\widehat{\mathbf{a}}_\ell^*(2^{-N}\Lambda)U^T f_G \approx U\mathcal{T}_\ell^{n*}(2^{-N}\Lambda)U^T f_G$$
$$= \mathcal{T}_\ell^{n*}(2^{-N}U\Lambda U^T)f_G = \mathcal{T}_\ell^{n*}(2^{-N}\mathcal{L})f_G \quad (2.3)$$

and for $2 \leq p \leq L$,

$$U\widehat{\mathbf{a}}_\ell^*(2^{-N+p-1}\Lambda)\widehat{\mathbf{a}}_0^*(2^{-N+p-2}\Lambda)\cdots\widehat{\mathbf{a}}_0^*(2^{-N}\Lambda)U^T f_G$$
$$\approx \mathcal{T}_\ell^{n*}(2^{-N+p-1}\mathcal{L})\mathcal{T}_0^{n*}(2^{-N+p-2}\mathcal{L})\cdots\mathcal{T}_0^{n*}(2^{-N}\mathcal{L})f_G. \quad (2.4)$$

Thus, by the iterative definition of Chebyshev polynomials, only matrix-vector multiplications are involved for computations of (2.3) and (2.4), and we don't need to obtain the full set of eigenvectors and eigenvalues of $\mathcal{L}$. Similarly, the wavelet frame reconstruction $\mathcal{W}^T$ can also be approximately computed.

3 Model and algorithm

3.1 Poisson noise removal of images on graphs

For a graph $G := \{V, E, \omega\}$, we formulate function $f_G : V \mapsto \mathbb{R}$ by a K-dimensional vector defined on the vertices. Let f_G be the observed noisy image on graph which is formulated as

$$f_G = u + \eta,$$

where η is the perturbation noise. We assume that f_G is corrupted by Poisson noise (see 1.2), i.e.

$$f_G \sim \mathbf{P}(u),$$

and the noise on each pixel is independent.

Then, given u, we have the likelihood of observing f_G

$$\mathbf{P}(f_G|u) = \prod_{i=0}^{K-1} \frac{u_i^{f_i} e^{-u_i}}{f_i!},$$

where u_i and f_i denote the ith element of u and f_G. By the properties of Poisson distribution, we obtain the mean and variance of f_G as follows

$$\mathbf{E}(f_G|u) = \mathbf{Var}(f_G|u) = u.$$

Let

$$\eta := f_G - u$$

be the "additive" random noise of the underlying image u on graph G. In the following, we approximate η by the normal distribution.

Given u, we have

$$\mathbf{E}(\eta|u) = \mathbf{E}(f_G|u) - u = 0, \quad \mathbf{Var}(\eta|u) = \mathbf{Var}(f_G|u) = u.$$

Then, we approximate η by the additive Gaussian noise $\mathcal{N}(0, u)$, i.e.,

$$\mathbf{P}(\eta|u) \propto \exp\left\{-\frac{1}{2}\eta^T \Sigma^{-1}\eta\right\}$$
$$= \exp\left\{-\frac{1}{2}(f_G - u)^T \Sigma^{-1}(f_G - u)\right\}, \quad (3.1)$$

where Σ is the covariance matrix. Due to the independence of noise at each element, we have

$$\Sigma = \mathrm{diag}(u).$$

We then take negative log of the normal distribution (3.1) and have

$$-\log \mathbf{P}(\eta|u) \propto \frac{1}{2}(f_G - u)^T \Sigma^{-1}(f_G - u).$$

Thus, by using the maximum likelihood estimates, we obtain the following fidelity term

$$\frac{1}{2}\|u - f_G\|_{\Sigma^{-1}}^2 := \frac{1}{2}\left\|\frac{u - f_G}{\sqrt{u}}\right\|_{\ell_2(G)}^2. \quad (3.2)$$

Here, the weighted ℓ_2 norm of a vector $\mathrm{x} \in \mathbb{R}^K$ is defined as $\|\mathrm{x}\|_{\Sigma^{-1}}^2 := \mathrm{x}^T \Sigma^{-1}\mathrm{x}$. The fidelity term (3.2) was introduced in [22,33] for Poisson data reconstruction. We here extend it to remove Poisson noise of images on graphs.

Under the assumption that the underlying solution is sparse in the wavelet frame domain, we propose the following model for removing Poisson noise of images on graphs

$$\min_u \frac{1}{2}\left\|\frac{u - f_G}{\sqrt{u}}\right\|_{\ell_2(G)}^2 + \lambda\|\mathcal{W}u\|_{\ell_1(G)}. \quad (3.3)$$

Here, the first term is a fitting term based on the noise characteristic and derived by the likelihood function discussed above; the second term is a regularization term, and λ is a parameter to balance the two terms.

Note that the division and square root operator in the fitting term are both element wise. In case $u = 0$, in practical implement, in order to guarantee the numerical stability, we add a very small positive constant (the fixed background image [3,6,30]) to u in model (3.3). To handle the unknown weight in the fitting term, following the line of [22], we apply the following iteration to solve the model.

Let $u_0 = f_G$. For $k = 1, 2, \ldots$, let

$$u^{k+1} := \arg\min_u \frac{1}{2}\left\|\frac{u - f_G}{\sqrt{u_k}}\right\|_{\ell_2(G)}^2 + \lambda\|\mathcal{W}u\|_{\ell_1(G)}. \quad (3.4)$$

The functional in (3.4) is an ℓ_1-regularized least-squares problem. Then, there are iterative solvers like the alternating direction method of multipliers (ADMM) [5,8,17] to obtain u^{k+1}, i.e.

$$\begin{cases} u_{k+1} = \arg\min_u \frac{1}{2}\left\|\frac{u - f_G}{\sqrt{u_k}}\right\|_{\ell_2(G)}^2 + \frac{\mu}{2}\|\mathcal{W}u - d_k + b_k\|_{\ell_2(G)}^2 \\ d_{k+1} = \arg\min_d \lambda\|d\|_{\ell_1(G)} + \frac{\mu}{2}\|\mathcal{W}u_{k+1} - d + b_k\|_{\ell_2(G)}^2 \\ b_{k+1} = b_k + \mathcal{W}u_{k+1} - d_{k+1} \end{cases}. \quad (3.5)$$

Let $\Sigma_k = \mathrm{diag}(u_k)$. Then, the solution to the first subproblem of (3.5) can be determined by solving the system of equations

$$(\Sigma_k^{-1} + \mu\mathcal{W}^T\mathcal{W})u_{k+1} = \mu\mathcal{W}^T(d_k - b_k) + \Sigma_k^{-1}f_G, \quad (3.6)$$

which, because of $\mathcal{W}^T\mathcal{W} = \mathcal{I}$, can be simplified to

$$(\Sigma_k^{-1} + \mu\mathcal{I})u_{k+1} = \mu\mathcal{W}^T(d_k - b_k) + \Sigma_k^{-1}f_G.$$

The second subproblem of (3.5) has a closed form solution, and d_{k+1} is given by the soft-shrinkage operator (see [5,8, 17])

$$d_{k+1} = \mathrm{sign}(\mathcal{W}u_{k+1} + b_k) \cdot \max(|\mathcal{W}u_{k+1} + b_k| - \lambda/\mu, 0), \quad (3.7)$$

where each operation is performed componentwisely.

Now, combining (3.6) and (3.7), we obtain Algorithm 1 for Poisson noise removal of images on graphs.

Algorithm 1 Algorithm for removal of Poisson noise on graphs

Initialize: $\varepsilon > 0$; $u_0 = f_G$; $d_0 = 0$; $b_0 = 0$; $\Sigma_0 = \mathrm{diag}(f_G)$
while $\|u_{k-1} - u_k\|_2 > \varepsilon$ or $k = 0$ **do**
$\quad u_{k+1} = (\Sigma_k^{-1} + \mu\mathcal{I})^{-1}(\mu\mathcal{W}^T(d_k - b_k) + \Sigma_k^{-1}f_G)$
$\quad d_{k+1} = \mathrm{sign}(\mathcal{W}u_{k+1} + b_k) \cdot \max(|\mathcal{W}u_{k+1} + b_k| - \lambda/\mu, 0)$
$\quad b_{k+1} = b_k + \mathcal{W}u_{k+1} - d_{k+1}$
$\quad \Sigma_{k+1} = \mathrm{diag}(u_{k+1})$
$\quad k = k + 1$
end while

3.2 Mixed Poisson–Gaussian noise

Previously, we discussed Poisson noise removal. In real graph data observation, there may exist other system-born noise
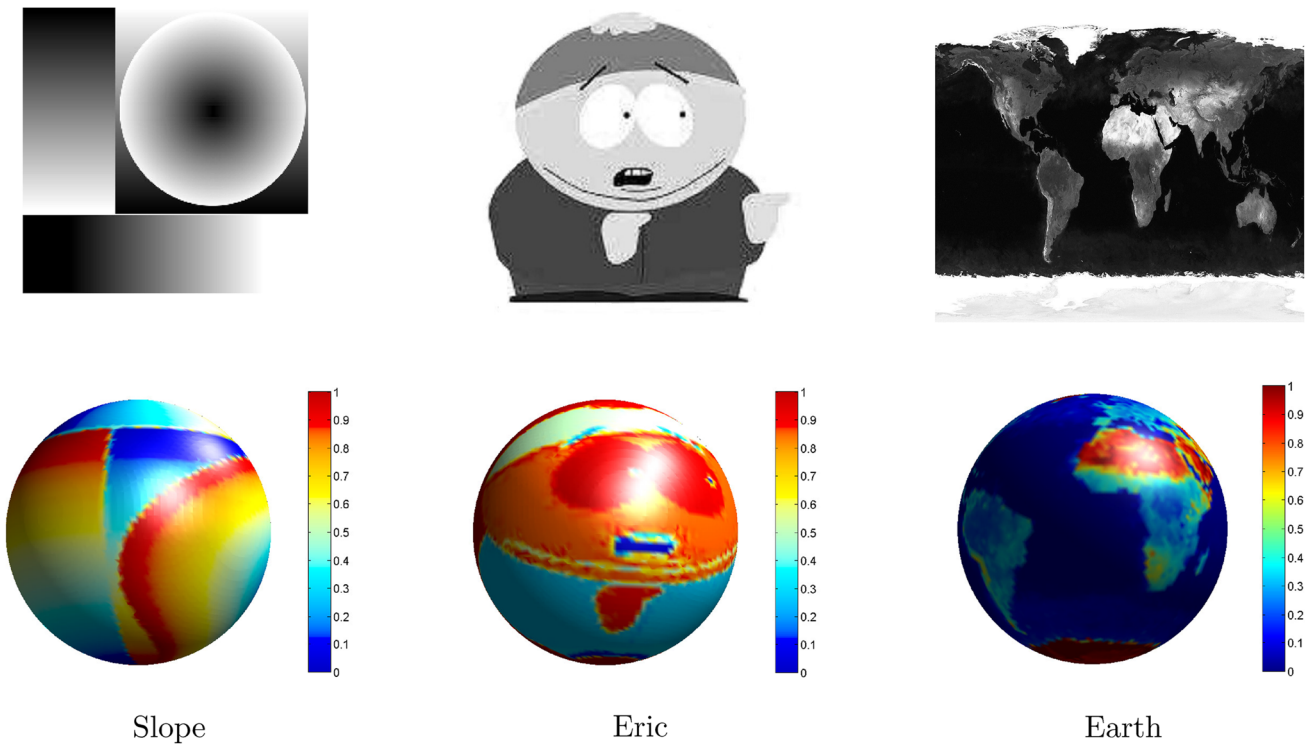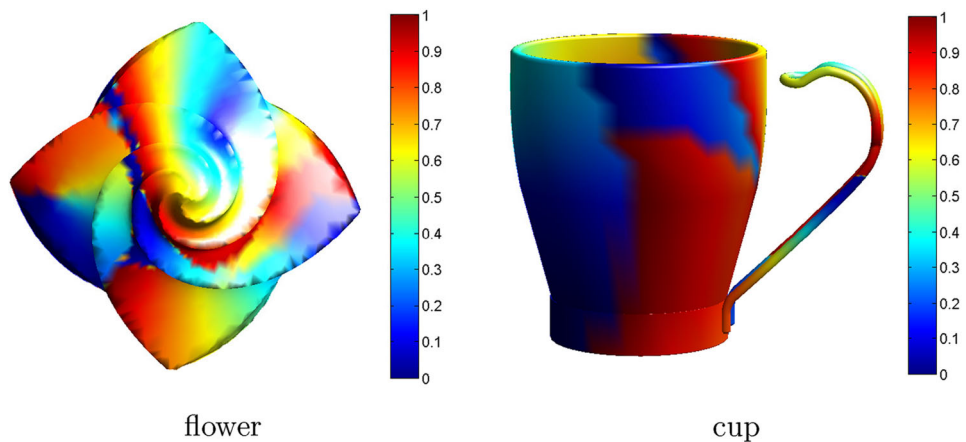
Fig. 1 The figure shows three images (*first row*), 'Slope', 'Eric' and 'Earth', which are mapped onto the graph of the unit sphere (*second row*)

Fig. 2 The figure shows two graphs, 'flower' and 'cup', which are generated by mapping the image 'Slope'

such as mixed Poisson–Gaussian. The observed image f_G on graph is corrupted by mixed Poisson–Gaussian noise following the distribution

$$f_G \sim \mathcal{P}(u) + \mathcal{N}(0, \sigma^2),$$

where σ^2 is the variance of additive Gaussian noise. Similar to the approach in Sect. 3.1, by applying the normal distribution (3.1) with covariance matrix $\Sigma = \mathrm{diag}(u) + \sigma^2 I$, the probability density function of the observed image data f_G can be approximated again. Then, we have a new weighted

ℓ_2 fidelity for removing mixed Poisson–Gaussian noise on graphs,

$$\frac{1}{2} \left\| \frac{u - f_G}{\sqrt{u + \sigma^2}} \right\|^2_{\ell_2(G)}.$$

Combining with the tight wavelet frame regularization, we propose the following denoising model

$$\min_u \frac{1}{2} \left\| \frac{u - f_G}{\sqrt{u + \sigma^2}} \right\|^2_{\ell_2(G)} + \lambda \|\mathcal{W}u\|_{\ell_1(G)}. \tag{3.8}$$
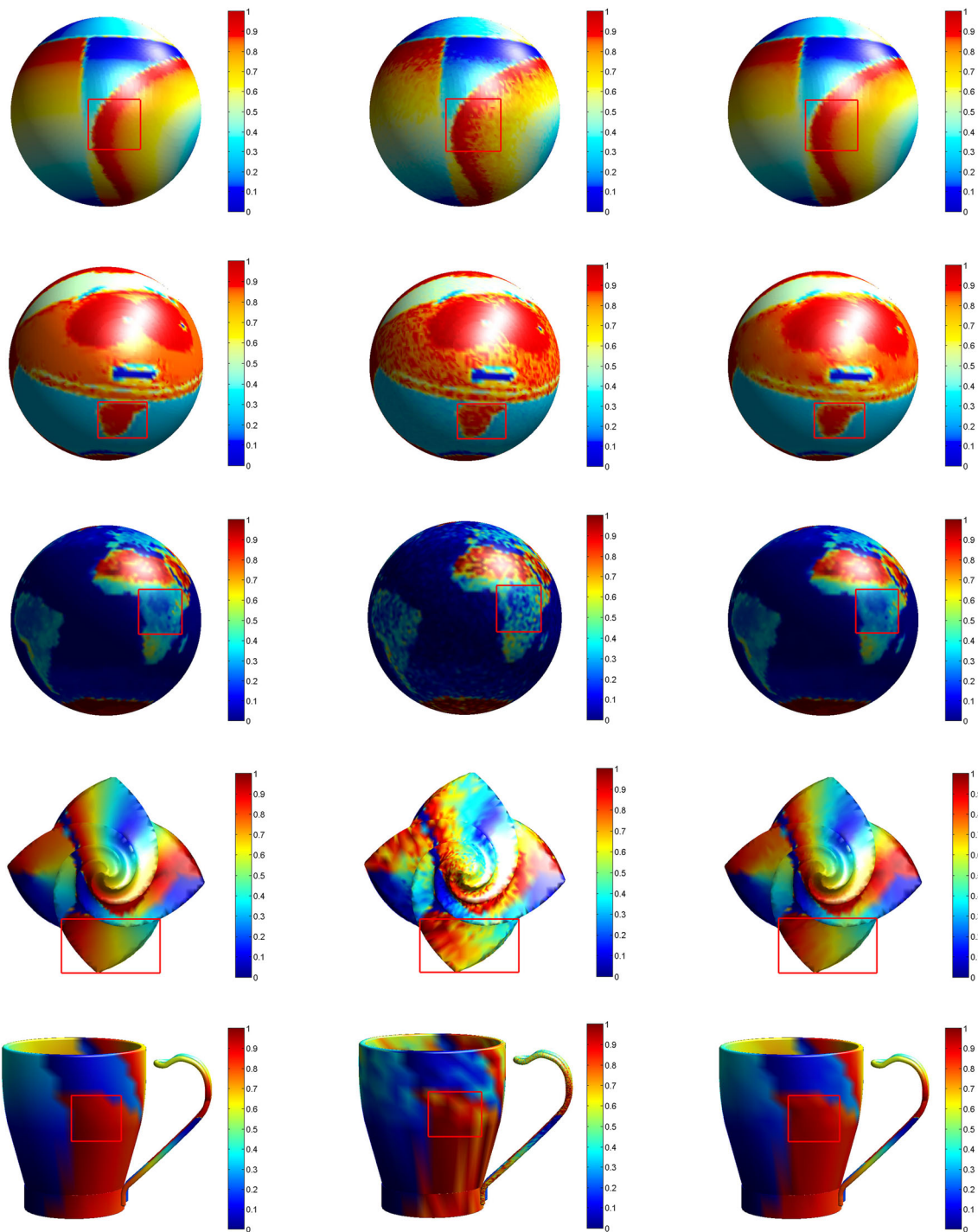
Fig. 3 Denoising results of the simulated noisy images on graphs corrupted by Poisson noise. From *left* to *right* noisy-free images on graphs, noisy images, denoised images. Parameters in the algorithm (Slope: $\lambda = 0.035$, $\mu = 0.35$; Eric: $\lambda = 0.035$, $\mu = 0.7$; Earth: $\lambda = 0.01$, $\mu = 0.1$; flower: $\lambda = 0.035$, $\mu = 0.875$; cup: $\lambda = 0.1$, $\mu = 1$)

Compared with model (3.3), here we extended the weighted ℓ_2 fidelity term to mixed Poisson–Gaussian noise by a small modification of the Poisson noise version. Thus, the corresponding algorithm solving (3.8) is similar to Algorithm 1 except adding σ^2 in estimation and updating covariance matrix.

Algorithm 2 Algorithm for removal of mixed Poisson–Gaussian noise on graphs

---

Initialize: $\varepsilon > 0$; $u_0 = f_G$; $d_0 = 0$; $b_0 = 0$; $\Sigma_0 = \mathrm{diag}(f_G) + \sigma^2 I$
while $\|u_{k-1} - u_k\|_2 > \varepsilon$ or $k = 0$ **do**
  $u_{k+1} = (\Sigma_k^{-1} + \mu\mathcal{I})^{-1}(\mu\mathcal{W}^T(d_k - b_k) + \Sigma_k^{-1}f_G)$
  $d_{k+1} = \mathrm{sign}(\mathcal{W}u_{k+1} + b_k) \cdot \max(|\mathcal{W}u_{k+1} + b_k| - \lambda/\mu, 0)$
  $b_{k+1} = b_k + \mathcal{W}u_{k+1} - d_{k+1}$
  $\Sigma_{k+1} = \mathrm{diag}(u_{k+1}) + \sigma^2 I$
  $k = k + 1$
end while

Table 1 Data summary and computational efficiency of Algorithm 1

Model	MSE ($\times 10^{-4}$)	SNR	NCC	Iterations	Time (s)
Slope	2.5106	31.9131	0.9962	25	7.1813
Eric	3.3796	33.4789	0.9906	20	5.8702
Earth	1.5627	29.0586	0.9930	30	5.6086
Flower	3.1208	30.9429	0.9968	25	4.0504
Cup	1.9568	33.2585	0.9969	35	6.0211

4 Numerical results and discussions

In the previous section, we discussed the model and algorithm for removing Poisson and mixed Poisson–Gaussian noise of images on graphs. In this section, we provide numerical experiments to test the performance of our method and compare with certain existing methods, such as the classical Laplacian smoothing method [4], the KL-divergence model [33] and Gong et al.' method [18]. Here, the KL-divergence model [33] and Gong et al.' model [18] are, respectively, formulated as

$$\min_u \mathbf{1}^T u + f_G{}^T \log(u) + \lambda\|\nabla u\|_{\ell_1(G)},$$

and

$$\min_u \|u - f_G\|^2_{\ell_1(G)} + \nu\|u - f_G\|^2_{\ell_2(G)} + \lambda\|\mathcal{W}u\|_{\ell_1(G)}.$$

In the first three experiments, the image functions defined on a graph are generated by mapping three images, 'Slope', 'Eric' and 'Earth', onto the unit sphere (see Fig. 1). Here, a unit sphere with 16,728 sampled vertices is selected as the graph. In the fourth and fifth experiments, two graphs named as 'flower' and 'cup' with 7919 and 10,840 sampled vertices are considered. The 'Slope' image function is mapped onto the graphs to test the performance of our approach (see Fig. 2). The two graphs are borrowed from the public 3D model database: http://3dmdb.com/.

In the computation of graph Laplacian, we choose parameter $\rho = 10$ in the weight function (2.1). For wavelet frame transform on graphs, we use the piecewise linear B-spline tight wavelet frame [26],

$$\widehat{a}_0(\xi) = \cos^2(\xi/2), \quad \widehat{a}_1(\xi) = \frac{1}{\sqrt{2}}\sin(\xi),$$
$$\widehat{a}_2(\xi) = \sin^2(\xi/2),$$

and we use the Chebyshev polynomials of degree 7 to approximate the masks, i.e., $n = 8$ in (2.3). For simplicity, we fix the level of wavelet frame transformation to 1, since using higher decomposition levels only slightly improves the denoising quality while the computation cost is noticeably increased.

The Algorithms 1 and 2 are implemented with MATLAB and experimented on a laptop with Intel Core i3-2310M (2.10 GHz) CPU and 6.0 GB RAM. The parameters in our algorithm are tuned to get the best visual outcome for the simulated noisy images on the graph. The denoised results $\overline{u}$ can be evaluated quantitatively by the mean squared error (MSE), the signal-to-noise ratio (SNR) and the normalized cross-correlation (NCC), which are defined by

$$\mathrm{MSE}(\overline{u}, u) := \frac{\|\overline{u} - u\|^2_{\ell_2(G)}}{K}, \quad \mathrm{SNR}(\overline{u}, u) := -20\log_{10}$$
$$\frac{\|\overline{u} - u\|_{\ell_2(G)}}{\|u\|_{\ell_2(G)}}, \mathrm{NCC}(\overline{u}, u) := \frac{\overline{u}^T u}{u^T u},$$

where u denotes the noisy-free images on graph, and K is the number of vertices.

4.1 Poisson noise removal

In this subsection, we test the performance of our approach for Poisson noise removal of images on graphs. Here, the clean image u is rescaled to an intensity ranging from 0 to 1200, and then the Poisson noise is added in MATLAB using the function 'poissrnd'. The denoised results are shown in Fig. 3. The denoised error, number of iterations and computational time for each image are given in Table 1.

Then we compare the results of our approach with other denoising methods. In Fig. 4, we visually show the difference between our method and the classical Laplacian smoothing method [4], the KL-divergence model [33] and Gong et al.' method [18]. It can be seen that our results preserve the local features better. Furthermore, we quantitatively compare these methods by MSE, SNR and NCC, see Tables 2, 3 and 4 for the results.

4.2 Mixed Poisson–Gaussian noise removal

In this subsection, we test the performance of mixed Poisson–Gaussian removal of images on graphs. Here, a Poisson noise is added to the original image first as in Sect. 4.1. Then, a
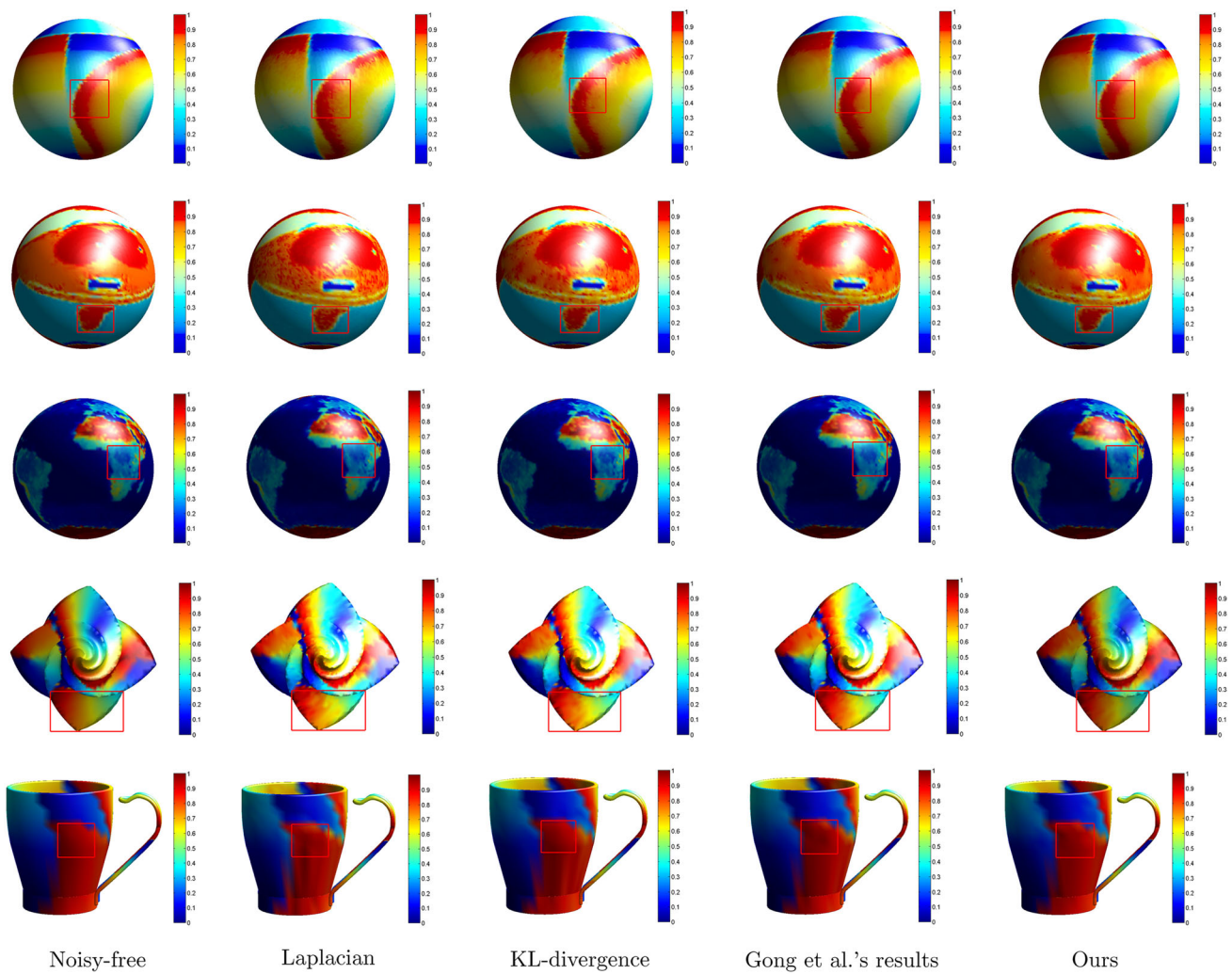
Fig. 4 Denoising results of the noisy images on graphs corrupted by Poisson noise. From *left* to *right* noisy-free images on graphs, Laplacian, KL-divergence, Gong et al.'s results, ours

Table 2 MSEs comparison for removal of Poisson noise ($\times 10^{-4}$)

Model	Laplacian	KL-divergence	Gong et al.	Ours
Slope	9.9995	3.3832	2.8153	2.5106
Eric	6.4938	4.8062	3.8114	3.3796
Earth	2.6659	2.1435	1.9636	1.5627
Flower	5.5115	4.5962	3.9658	3.1208
Cup	7.5561	3.4574	2.5424	1.9568

Table 3 SNRs comparison for removal of Poisson noise

Model	Laplacian	KL-divergence	Gong et al.	Ours
Slope	25.8827	30.6176	31.4156	31.9131
Eric	31.8352	31.9496	32.9567	33.4789
Earth	26.7390	27.6862	28.0668	29.0586
Flower	28.4729	29.2616	29.9023	30.9429
Cup	27.3911	30.7866	32.1215	33.2585

Gaussian noise with distribution $\mathcal{N}(0, \sigma^2)$ is added to the image. We choose $\sigma = 6$. The denoised results are shown in Fig. 5, and the denoised error, number of iterations and computational time for each image are given in Table 5.

In the end, we compare the results of our approach with the Laplacian smoothing method [4], the KL-divergence model [33] and Gong et al.' method [18] both visually and quantitatively. Figure 6 shows that our results preserve most textures and edges on graphs better. Furthermore, we compare these

Table 4 NCCs comparison for removal of Poisson noise

Model	Laplacian	KL-divergence	Gong et al.	Ours
Slope	0.9903	0.9959	0.9961	0.9962
Eric	0.9866	0.9890	0.9891	0.9906
Earth	0.9902	0.9903	0.9923	0.9930
Flower	0.9954	0.9971	0.9968	0.9976
Cup	0.9952	0.9925	0.9960	0.9969

methods by MSE, SNR and NCC, see Tables 6, 7 and 8 for the results.

5 Conclusion

In this paper, we considered Poisson and mixed Poisson–Gaussian noise removal of images on graphs. Based on
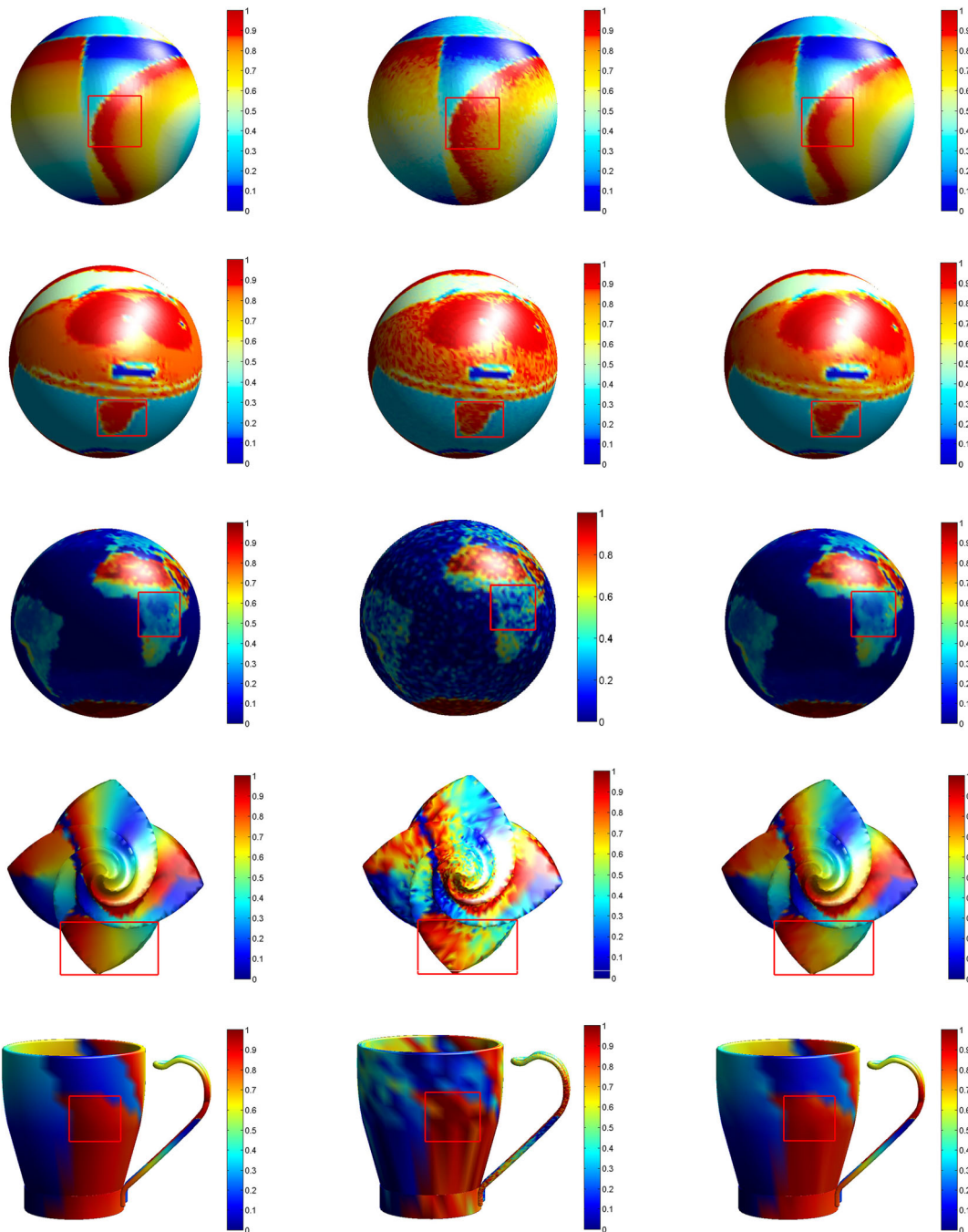

Fig. 5 Denoising results of the noisy images on graphs corrupted by mixed Poisson–Gaussian noise. From *left* to *right* noisy-free images on graphs, noisy images on graphs, denoised images on graphs. Parameters in the algorithm (Slope: $\lambda = 0.035$, $\mu = 0.35$; Eric: $\lambda = 0.035$, $\mu = 0.7$; Earth: $\lambda = 0.01$, $\mu = 0.1$; flower: $\lambda = 0.035$, $\mu = 0.875$; cup: $\lambda = 0.1$, $\mu = 1$)

Table 5 Data summary and computational efficiency of Algorithm 2

Model	MSE ($\times 10^{-4}$)	SNR	NCC	Iterations	Time(s)
Slope	2.6000	31.7612	0.9957	40	10.7767
Eric	3.4415	33.4001	0.9899	50	13.2963
Earth	1.6804	28.7431	0.9933	30	6.0435
Flower	3.2060	30.8260	0.9976	25	4.2854
Cup	2.0921	32.9682	0.9967	35	6.3073

Table 6 MSEs comparison for removal of mixed Poisson–Gaussian noise ($\times 10^{-4}$)

Model	Laplacian	KL-divergence	Gong et al.	Ours
Slope	9.9992	3.4536	2.8471	2.6000
Eric	6.7159	4.8291	3.9092	3.4415
Earth	2.8232	2.3762	2.0820	1.6804
Flower	5.5976	4.9709	4.0719	3.2060
Cup	7.6861	3.7854	2.5553	2.0921

the statistical characteristic of noise, we approximated the probability density function of observed images by the normal distributions. Then, a fidelity term was derived by the likelihood function. In addition, under the assumption that the underlying image in the wavelet frame domain is sparse, we proposed a variational model to denoise the

images on graphs. We then applied the popular iterative algorithm ADMM to solve the model. Finally, we demonstrated the numerical experiments to verify the practicability and effectiveness of our approach, and compared with the classical Laplacian smoothing method [4], the KL-divergence
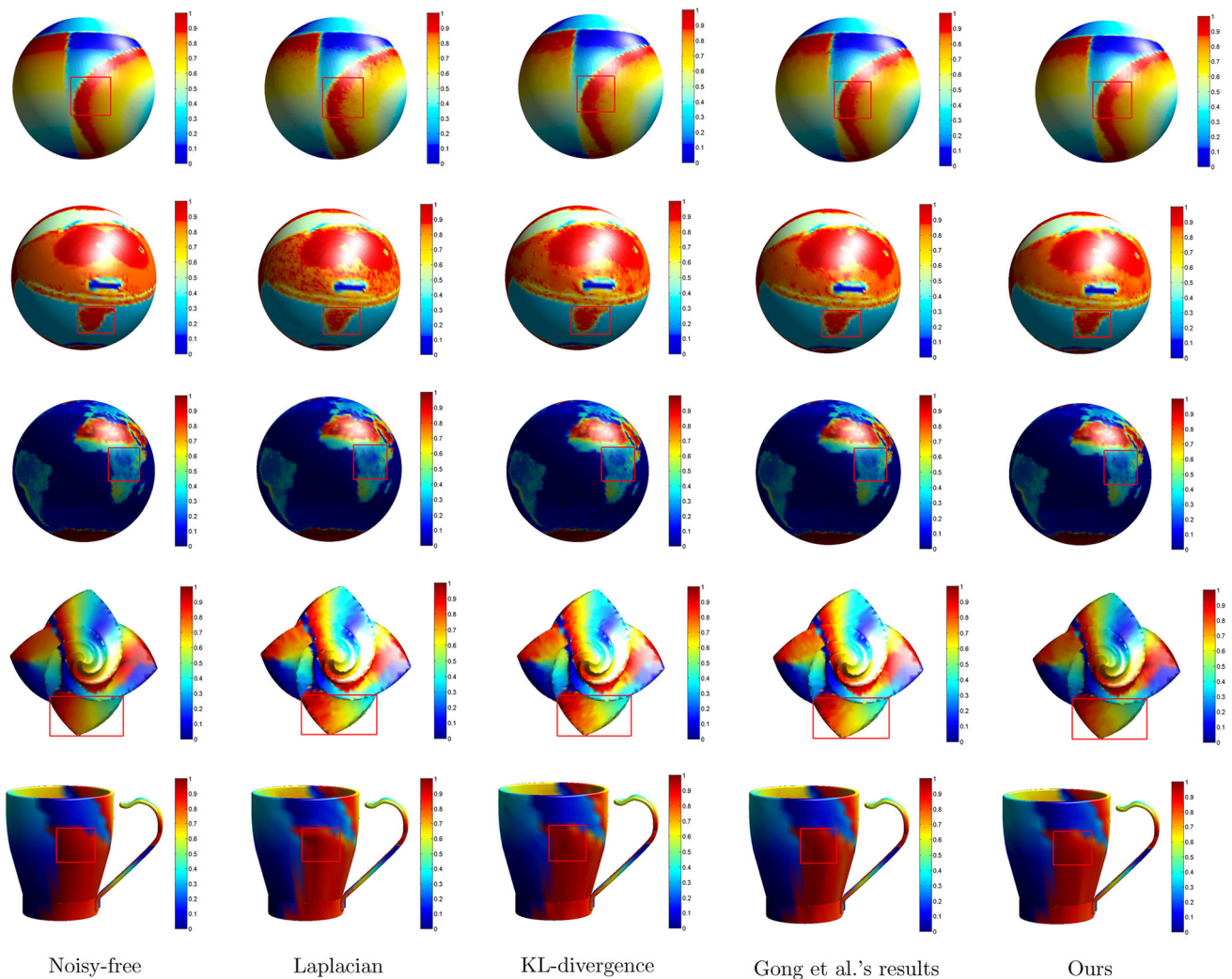

| Noisy-free | Laplacian | KL-divergence | Gong et al.'s results | Ours |

Fig. 6 Denoising results of the noisy images on graphs corrupted by mixed Poisson–Gaussian noise. From *left* to *right* noisy-free images on graphs, Laplacian, KL-divergence, Gong et al.'s results, ours

Table 7 SNRs comparison for removal of mixed Poisson–Gaussian noise

Model	Laplacian	KL-divergence	Gong et al.	Ours
Slope	25.7891	30.5283	31.3669	31.7612
Eric	30.4966	31.9289	32.8467	33.4001
Earth	26.4899	27.2385	27.8126	28.7431
Flower	28.4055	28.9213	29.7876	30.8260
Cup	27.3170	30.3930	32.0997	32.9682

Table 8 NCCs comparison for removal of mixed Poisson–Gaussian noise

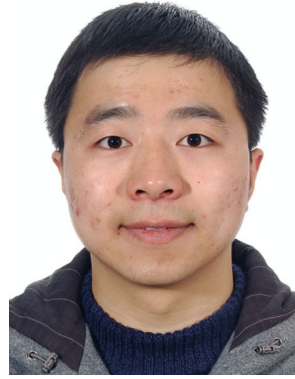| Model	Laplacian	KL-divergence	Gong et al.	Ours
Slope	0.9907	0.9954	0.9957	0.9963
Eric	0.9868	0.9887	0.9899	0.9890
Earth	0.9900	0.9903	0.9923	0.9933
Flower	0.9965	0.9975	0.9976	0.9978
Cup	0.9927	0.9958	0.9966	0.9967

model [33] and Gong et al.' method [18]. The results on some image denoising tasks indicate the effectiveness of our method.

References

1. Belkin, M., Niyogi, P.: Towards a theoretical foundation for Laplacian-based manifold methods. In: Proceedings of the 18th Annual Conference on Learning Theory (COLT), pp. 486–500. Springer, (2005)
2. Benninghoff, H., Garcke, H.: Segmentation and restoration of images on surfaces by parametric active contours with topology changes. J. Math. Imaging Vis. **55**(1), 105–124 (2016)
3. Bertero, M., Boccacci, P., Talenti, G., Zanella, R., Zanni, L.: A discrepancy principle for Poisson data. Inverse Probl. **26**(10), 105004–105023 (2010)
4. Botsch, M., Kobbelt, L., Pauly, M., Alliez, P., Levy, B.: Polygon Mesh Processing. AK Peters, Natick (2010)
5. Boyd, S., Parikh, N., Chu, E., et al.: Distributed optimization and statistical learning via the alternating direction method of multipliers. Foundations and Trends®. Mach. Learn. **3**(1), 1–122 (2011)
6. Sawatzky, A., Brune, C., Kösters, T., Wübbeling, F., Burger, M.: EM-TV Methods for Inverse Problems with Poisson Noise. In: Level Set and PDE Based Reconstruction Methods in Imaging, vol 2090, pp. 71–142. Springer, Cham (2013)
7. Cai, J.-F., Dong, B., Osher, S., Shen, Z.: Image restoration: total variation, wavelet frames, and beyond. J. Am. Math. Soc. **25**(4), 1033–1089 (2012)
8. Cai, J.-F., Osher, S., Shen, Z.: Split Bregman methods and frame based image restoration. Multiscale Model. Simul. SIAM Interdiscip. J. **8**(2), 337–369 (2009)
9. Chan, R.H., Chen, K.: Multilevel algorithm for a Poisson noise removal model with total variation regularization. Int. J. Comput. Math. **84**(8), 1183–1198 (2007)
10. Coifman, R.R., Lafon, S.: Diffusion maps. Appl. Comput. Harmon. Anal. **21**(1), 5–30 (2006)
11. Csiszár, I.: Why least squares and maximum entropy? An axiomatic approach to inference for linear inverse problems. Ann. Stat. **19**(4), 2032–2066 (1991)
12. Dong, B.: Sparse representation on graphs by tight wavelet frames and applications. Appl. Comput. Harmon. Anal. **42**(3), 452–479 (2017)
13. Dong, B., Jiang, Q.T., Liu, C.Q., Shen, Z.: Multiscale representation of surfaces by tight wavelet frames with applications to denoising. Appl. Comput. Harmon. Anal. **41**(2), 561–589 (2016)
14. Dong, B., Shen, Z.: MRA-based wavelet frames and applications. In: Zhao, H. (ed.) IAS Lecture Notes Series, Summer Program on The Mathematics of Image Processing. Park City Mathematics Institute, Salt Lake City, (2010)
15. El Ouafdi, A.F., Ziou, D.: Global diffusion method for smoothing triangular mesh. Vis. Comput. **31**(3), 295–310 (2015)
16. Giné, E., Koltchinskii, V.: Empirical graph Laplacian approximation of Laplace–Beltrami operators: large sample results. IMS Lect. Notes Monogr. Ser. **51**, 238–259 (2006)
17. Goldstein, T., Osher, S.: The split Bregman algorithm for L1-regularized problems. SIAM J. Imaging Sci. **2**(2), 323–343 (2009)
18. Gong, Z., Shen, Z., Toh, K.: Image restoration with mixed or unknown noises. Multiscale Model. Simul. **12**(2), 458–487 (2014)
19. Hein, M. Audibert, J.-Y., Von Luxburg, U.: From graphs to manifolds-weak and strong pointwise consistency of graph Laplacians. In: Proceedings of the 18th Annual Conference on Learning Theory, pp. 470–485. Springer (2005)
20. Jain, P., Tyagi, V.: An adaptive edge-preserving image denoising technique using tetrolet transforms. Vis. Comput. **31**(5), 657–674 (2015)
21. Le, T., Chartrand, R., Asaki, T.J.: A variational approach to reconstructing images corrupted by Poisson noise. J. Math. Imaging Vis. **27**(3), 257–263 (2007)
22. Li, J., Shen, Z., Yin, R., Zhang, X.: A reweighted ℓ^2 method for image restoration with Poisson and mixed Poisson–Gaussian noise. Inverse Probl. Imaging **9**(3), 875–894 (2015)
23. Luisier, F., Blu, T., Unser, M.: Image denoising in mixed Poisson–Gaussian niose. IEEE Trans. Image Process. **20**(3), 696–708 (2011)
24. Mason, J.C., Handscomb, D.C.: Chebyshev Polynomials. CRC Press, Boca Raton (2002)
25. Niyobuhungiro, J., Setterqvist, E.: A new reiterative algorithm for the Rudin–Osher–Fatemi denoising model on the graph. In: Proceedings of the 2nd International Conference on Intelligent Systems and Image Processing 2014, pp. 81–88. (2014)
26. Ron, A., Shen, Z.: Affine systems in $L_2(\mathbb{R}^d)$: the analysis of the analysis operator. J. Funct. Anal. **148**(2), 408–447 (1997)
27. Ron, A., Shen, Z.: Compactly supported tight affine spline frames in $L_2(\mathbb{R}^d)$. Math. Comput. **67**(221), 191–207 (1998)
28. Rudin, L., Osher, S., Fatemi, E.: Nonlinear total variation based noise removal algorithms. Phys. D **60**(1–4), 259–268 (1992)
29. Rusu, R.B., Marton, Z.C., Blodow, N., Dolha, M., Beetz, M.: Towards 3D Point cloud based object maps for household environments. Robot. Auton. Syst. **56**(11), 927–941 (2008)
30. Shepp, L.A., Vardi, Y.: Maximum likelihood reconstruction in positron emission tomography. IEEE Trans. Med. Imaging **1**(2), 113–122 (1982)
31. Singer, A.: From graph to manifold Laplacian: the convergence rate. Appl. Comput. Harmon. Anal. **21**(1), 128–134 (2006)

32. Shuman, D.I., Vandergheynst, P., Frossard, P.: Chebyshev polynomial approximation for distributed signal processing. In: International Conference on Distributed Computing in Sensor Systems and Workshops, pp. 1–8. (2011)

33. Staglianò, A., Boccacci, P., Bertero, M.: Analysis of an approximate model for Poisson data reconstruction and a related discrepancy principle. Inverse Probl. **27**(12), 125003 (2011)

34. Yang, J., Stahl, D., Shen, Z.: An analysis of wavelet frame based scattered data reconstruction. Appl. Comput. Harmon. Anal. **42**(3), 480–507 (2017)

35. Yang, J., Wang, C.: A wavelet frame approach for removal of mixed Gaussian and impulse noise on surfaces. Inverse Probl. Imaging. **11**(5), 1 (2017). doi:10.3934/ipi.2017037

36. Zhang, B., Fadili, J.M., Starck, J.-L.: Wavelets, ridgelets, and curvelets for Poisson noise removal. IEEE Trans. Image Process. **17**(7), 1093–1108 (2008)

37. Zhang, H., Wu, C., Zhang, J., Deng, J.: Variational mesh denoising using total variation and piecewise constant function space. IEEE Trans. Vis. Comput. Graph. **21**(7), 873–886 (2015)

38. Zosso, D., Osting, B., Osher, S.: A dirichlet energy criterion for graph-based image segmentation. In: IEEE 15th International Conference on Data Mining Workshops, pp. 821–830. (2015)

Jianbin Yang received his B.S. degree in applied mathematics from Yang Zhou University in 2005, and Ph.D. in applied mathematics from Zhejiang University in 2010. He worked as a research fellow at the Department of Mathematics, National University of Singapore from 2013 to 2014. He is currently an associate professor in mathematics in Hohai University. His research interests include image processing, wavelet analysis and its applications.

Cong Wang received his B.S. degree in automation from College of Internet of Things (IOT) Engineering, Hohai University, and the M.S. degree in mathematics from College of Science, Hohai University in 2014 and 2017, respectively. He is currently a Ph.d. candidate in Xidian University. His research interests include wavelet analysis and surface reconstruction.